*Mapana – Journal of Sciences*
2026, Vol. 25, No. 1, *33-48*
ISSN 0975-3303 | https://doi.org/10.12723/mjs.76.3

# Comparative studies of photophysical properties of Indole molecules

Vijayalaxmi Mallayya*, Srinath More*, Omnath Patil*, Nagesh G. Y†, S. M. Hanagodimath*

## Abstract

In this study, a comparative investigation of 5-methyl-3-phenyl-1H-indole-2-carbohydrazide and 5-chloro-3-phenyl-1H-indole-2-carbohydrazide is presented. Molecular structures were determined, and their UV–visible absorption spectra along with $^{1}H$ and $^{13}C$ NMR chemical shift values were systematically analysed. The effect of pure solvents on the spectral properties was examined using solvatochromic theories. Ground- and excited-state dipole moments were estimated through the solvatochromic approach. The higher dipole moments observed in the excited state, together with the red shift in the emission spectra, suggest that the singlet excited state exhibits intramolecular charge-transfer (ICT) character. In addition, theoretical studies were performed using density functional theory (DFT) at the CAM-B3LYP/6-31+G(d,p) level with Gaussian software. Additionally, the energies of the highest occupied and lowest unoccupied molecular orbitals (HOMO and LUMO), as well as the global chemical reactivity descriptors (GCRD), were assessed at the DFT/B3LYP/6-311+G(d,p) level. Additionally, molecular electrostatic potential (MEP) maps were constructed to determine regions most susceptible to electrophilic and nucleophilic attack. The experimentally measured ground-state dipole moments (1.67 D and 13.1 D) were discovered to be greater than corresponding theoretical values (1.11 D and 6.44 D).

**Keywords:** Dipole moment; Indole-based compounds; Solvatochromic analysis; Gaussian 16W calculations

* Department of Physics, Gulbarga University, Kalaburagi 585106. India; mallayyalaxmi49@gmail.com, omnathpatil@gmail.com, smhmath@rediffmail.com

† Department of Chemistry, Guru Nanak First Grade College, Bidar, Karnataka, India; nageshyernale@gmail.com

## 1. Introduction

Indole derivatives are known to possess diverse biological activities such as anti-inflammatory, antiviral, anticancer, antimalarial, antioxidant, anti-HIV, antitubercular, antimicrobial, antidiabetic, and anticholinesterase properties. These diverse activities have stimulated significant research interest in the synthesis of novel indole-based compounds. Structurally, indole, also known as benzopyrrole, consists of a benzenoid nucleus with 10 π-electrons (8 from the double bonds and two from the nitrogen lone pair), which imparts aromatic character. Similar to benzene, indole undergoes electrophilic substitution reactions readily due to extensive π-electron delocalization [1].

Indole is an essential heterocyclic scaffold and forms structural basis of several biologically significant compounds, including lysergic acid diethylamide (LSD), strychnine, and various plant alkaloids. In its pure form, indole is a colourless crystalline solid with a characteristic odour. Because biologically active pharmacophores contain indole nucleus, it has made a privileged structure in medicinal chemistry, leading to design and synthesis of numerous indole derivatives for pharmacological screening. Many natural products also contain the indole core, such as the amino acid tryptophan and plant hormone indole-3-acetic acid, formed by tryptophan degradation in higher plants. Owing to these features, indole derivatives continue to receive significant attention for their broad spectrum of biological and clinical applications. This work aims to highlight and summarize the pharmacological relevance of indole-based compounds [3].

When one or more carbon atoms in the ring are replaced with heteroatoms, the resulting cyclic structure is known as a heterocyclic molecule. "Heteroatoms" are the non-carbon atoms that make up these rings. Bicyclic heterocyclic compounds in which a pyrrole ring is fused to a benzene ring at the α- and β-positions are referred to as indoles. In an indole, the benzene and pyrrole rings share a common double bond, forming a heterocyclic system with ten π-electrons contributed by four double bonds and the nitrogen atom's lone pair. Indole is a significant heterocyclic structure because it is a component of amino acid tryptophan seen in proteins, assists as core structure for drugs such as indomethacin, and forms the backbone of indole alkaloids—naturally occurring biologically active compounds in plants, encompassing strychnine as well as LSD.

The reaction kinetics "of indole (1a), N-methylindole (1b), 5-methoxyindole (1c), and 5-cyanoindole (1d) with a series of reference benzhydryl cations were examined in acetonitrile and/or dichloromethane. The second-order rate constants for these reactions showed a linear correlation with the electrophilicity parameter (E) of the benzhydryl cations. This relationship allows the calculation of nucleophilicity parameters, N and

s, for 1a–d using the linear free energy equation: log k (20 °C) = *s* (N + E) (*Acc. Chem. Res. 2003, 36, 66*). These nucleophilicity parameters successfully describe the reactivity of 1a–d with 4,6-dinitrobenzofuroxan (2), a neutral, highly electrophilic heteroaromatic compound whose electrophilicity (E) has recently been determined. Based on this framework, the kinetics of 2 with various indole derivatives were investigated in acetonitrile, establishing a reactivity ranking for this class of π-rich carbon nucleophiles across a broad nucleophilicity scale (N). Notably, plotting the measured N values against the pKa ($H_2O$) for protonation at the C-3 position of 5-X-substituted indoles and 5-X-substituted 2-methylindoles revealed two linear, parallel correlations. This divergence indicates that the 2-methyl group introduces steric hindrance, impeding the approach of 2 toward the C-3 position. The N vs. p*Ka*($H_2O$) correlation for 5-X-substituted indoles provides a practical method to estimate the C-3 basicity of indoles whose acidity constants cannot be directly measured in strongly acidic aqueous media. [2] The indole framework is a key" structural element in numerous natural and synthetic compounds with notable biological activity. This review highlights recent advancements in the chemical, biological, and pharmacological properties of important indole derivatives, emphasizing their significance in drug discovery and analytical applications [3-5].

## 2. Materials and methods

The indole derivative namely "5-methyl-3-phenyl-1*H*-indol-2-carbohydrazide [MPIC]" and "5-Chloro-3-phenyl-1H-indol-2-carbohydrazide [CPIC]" was synthesized by using reported method [7]. The molecular structure of the fluorescent molecule is given in Fig.1(a) and (b). The solvents used for the present work, methanol, ethanol, propanol, pentanol, hexanol, heptanol, nonanol, octanol, butanol, decanol, reagents and chemicals required for the synthesis and analysis were bought from Sigma Aldrich Pvt Ltd. They were utilized to obtain AR-grade. The required solutions were prepared at a fixed solute concentration ($1x10^{-5}$ M/L). In order to minimize the effect of self-absorption, the concentration of solute was kept sufficiently low to obtain spectroscopic grade solvents. Absorption and emission spectra were recorded on a PG Inst. Ltd., model T-90+, UV–Visible absorption spectrophotometer and fluorescence spectra on FP-8300 fluorescence spectrometer [6-11].

## 3. Theoretical background

### 3.1. Estimation of Ground ($\mu_g$) and Excited State ($\mu_e$) Dipole Moments

The influence of solvent polarity on the indole derivative was studied by using Solvatochromic shift method in solute-solvent mixtures. This method relies on "Onsager's reaction field theory, describing non-specific

electrostatic interactions. The independent equations used for estimating ground and excited state dipole moments of indole derivatives in several solvent of varying refractive index ($n$) as well as dielectric constant" ($\varepsilon$) are [12-16].

Lippert-Mataga Equation

$$\bar{\nu}_a - \bar{\nu}_f = m_1 F_1(\varepsilon, n) + Constant \quad (1)$$

Bakhshiev"s equation

$$\bar{\nu}_a - \bar{\nu}_f = m_2 F_2(\varepsilon, n) + Constant \quad (2)$$

Kawski Chamma Vialette's equation

$$\frac{\bar{\nu}_a + \bar{\nu}_f}{2} = -m_3 F_3(\varepsilon, n) + Constant—, \quad (3)$$

where **a** and **f** represent the absorption and fluorescence maxima wavenumbers in $cm^{-1}$ respectively, and solvent polarity functions $F_1$, $F_2$, and $F_3$ are provided below.

$$F_1(\varepsilon, n) = \left[\frac{\varepsilon - 1}{2\varepsilon + 1} - \frac{n^2 - 1}{2n^2 + 1}\right] \quad (4)$$

$$F_2(\varepsilon, n) = \left[\frac{\varepsilon - 1}{\varepsilon + 2} - \frac{n^2 - 1}{n^2 + 2}\right] \frac{(2n^2 + 1)}{(n^2 + 2)} \quad (5)$$

$$F_3(\varepsilon, n) = \frac{2n^2 + 1}{2(n^2 + 2)} \left[\frac{\varepsilon - 1}{\varepsilon + 2} - \frac{n^2 - 1}{n^2 + 2}\right] + \frac{3(n^4 - 1)}{2(n^2 + 2)^2} \quad (6)$$

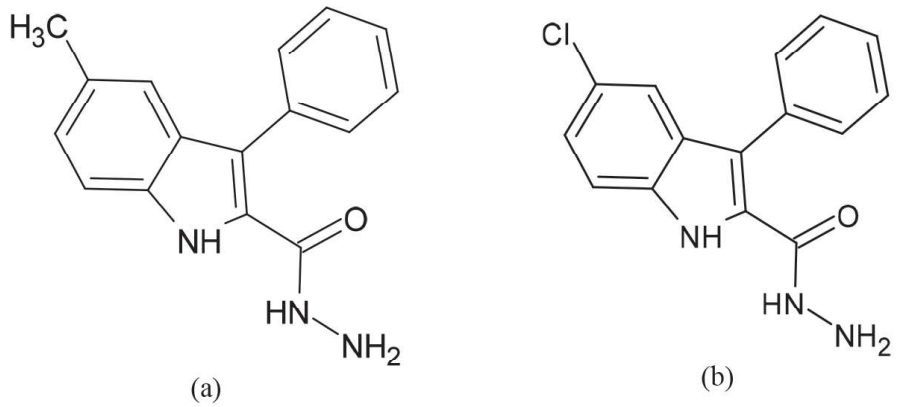


**Figure 1:** Molecular structure of (a) MPIC and (b) CPIC molecule

The meanings of **ε** and **n** are as usual. The plots of $\bar{\nu}_a - \bar{\nu}_f$ v/s $F_1(\text{Ɛ}, n)$, $F_2(\text{Ɛ}, n)$ and $\frac{\bar{\nu}_a + \bar{\nu}_f}{2}$ versus $F_3(\text{Ɛ}, n)$ have been plotted respectively and the slopes $m_1$, $m_2$ and $m_3$ are obtained respectively, as shown below.

$$m_1 = \frac{2(\mu_e - \mu_g)^2}{hca_0^3} \quad (7)$$

$$m_2 = \frac{2(\mu_e - \mu_g)^2}{hca_0^3} \quad (8)$$

$$m_3 = \frac{2(\mu_e^2 - \mu_g^2)}{hca_0^3} \quad (9)$$

The dipole moments $\mu_e$ and $\mu_g$ indicate the excited-state and ground-state dipole moments of an indole molecule. The letters **'a'** denote the Onsager's cavity radius of the solute molecule, where **'h'** is Planck's constant and **'c'** is the velocity of light. Edward [17] uses the microscopic increment method to estimate **'a'** value. The following equations (10) and (11) are obtained on the basis of equations (8) and (9)

$$\mu_g = \frac{m_3 - m_2}{2}\left[\frac{hca_0^3}{2m_2}\right]^{\frac{1}{2}} \quad (10)$$

$$\mu_e = \frac{m_3 + m_2}{2}\left[\frac{hca_0^3}{2m_2}\right]^{\frac{1}{2}} \quad (11)$$

### 3.2. Molecular-Microscopic Solvent polarity Parameter ($E_T^N$)

Utilizing spectral features, H-bonding or polarization dependency can be investigated. $E_T^N$ Reichardt [18] suggested a connection between $E_T^N$and spectral shift. In their different theories, Reichardt and Ravi et al. suggested a connection among Stokes shift and $E_T^N$. Consequently, eq$^n$ (12) is derived

$$\overline{\nu}_a - \overline{\nu}_f = 11307.6\left[\frac{\Delta\mu^2 a_B^3}{\Delta\mu_B^2 a^3}\right] E_T^N + Constant, \quad (12)$$

where $\Delta\mu$ = 9 D and $a_B$ = 6.2 Å are the change in dipole moment on excitation. The change in dipole moment can be evaluated from the slope of the stokes shift versus $E_T^N$ plot and is given by equation (13)[18].

$$\Delta\mu = \mu_e - \mu_g = \sqrt{\frac{m \times 81}{\left[\frac{6.2}{a}\right]^3 X\ 11307.6}}, \quad (13)$$

where m is the slope of the linear plot of $E_T^N$ Vs Stokes shift.

## 4. Results and Discussions

### 4.1. Estimation of ground and excited- state dipole moments

Absorption and fluorescence spectra "of synthesized probes were measured

repeatedly in solvents of different polarities for making sure reproducibility and minimize experimental errors. The verified spectra are presented in Figures 2 & 3, respectively [19-25].

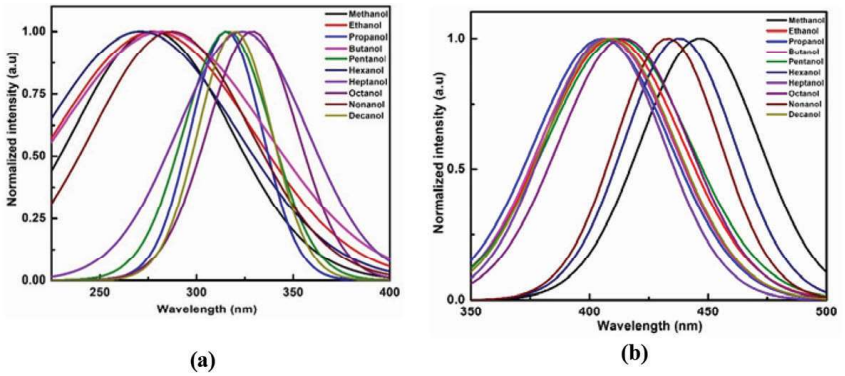


**Figure 2:** (a) Absorption spectra and (b) Fluorescence spectra of MPIC in selected solvents

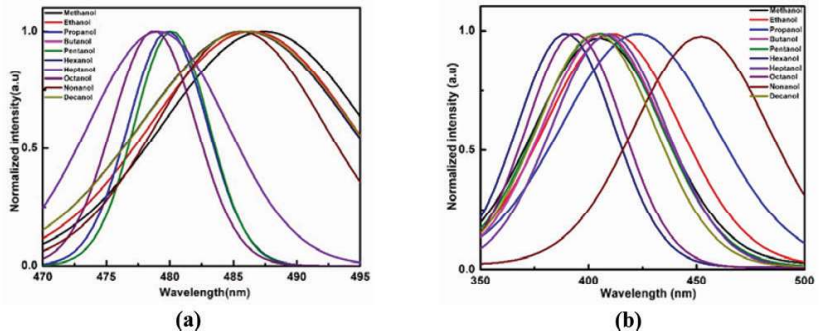


**Figure 3:** (a) Absorption spectra and (b) Fluorescence spectra of CPIC in selected solvents

The normalized absorption and emission spectra of MPIC and CPIC in various solvents are shown in Figures 2(a) and (b) and 3(a) and (b), correspondingly. The absorption and emission wavelengths range from 273 to 329 nm and 408 to 419 nm for MPIC, and 273 to 329 nm and 399 to 414 nm for CPIC, depending on the solvent [26]. A comparison of the spectra shows that the emission bands exhibit a larger shift than the absorption bands. This shift in the absorption and emission maxima is attributed to the dielectric constants of the solvents used. For recording emission spectra, samples were excited at their respective absorption maxima [27]. Longest wavelength absorption band corresponds to the intramolecular charge-transfer (ICT) transition, which also defines the excitation maxima. Table 1(a)–(b) summarizes the arithmetic mean, Stokes shift, and emission and absorption maxima of derivatives in different solvents. Switching the solvent from polar aprotic ethanol to methanol leads to noticeable spectral shifts in the absorption spectra, with values of 279nm for MPIC and 276, 275, &269nm for CPIC. Similarly, emission maxima shift from 413nm for MPIC and 415, 401, & 405nm for CPIC. These changes indicate that variations in solvent

polarity and hydrogen-bonding capabilities influence the ground-state energy distribution of these derivatives. A comparison of emission maxima in ethanol and methanol further suggests that hydrogen-bonding properties of the solvents have a more pronounced effect on emission behaviour of both derivatives. Ethanol and methanol display Stokes shifts of" 35842cm$^{-1}$,36231 cm$^{-1}$, & 36363 cm$^{-1}$,37174 cm$^{-1}$, respectively [28-35].

**Table 1:** (a) and (b) The absorption maxima, emission maxima, corresponding wave- numbers, Stokes shift and arithmetic stokes shifts in cm$^{-1}$ for (a) MPIC and (b) CPIC in alcohols.

| **Solvents** | $\bar{\nu}_a$ | $\bar{\nu}_f$ | $\bar{\nu}_a - \bar{\nu}_f$ | $\left(\frac{\bar{\nu}_a + \bar{\nu}_f}{2}\right)$ |
|---|---|---|---|---|
| Methanol | 36231 | 24096 | 12135 | 30163 |
| Ethanol | 35842 | 24213 | 11629 | 30027 |
| Propanol | 31746 | 24390 | 7356 | 28068 |
| Butanol | 35460 | 24509 | 10951 | 29984 |
| Pentanol | 31746 | 24330 | 7416 | 28038 |
| Hexanol | 36630 | 24390 | 12240 | 30510 |
| Heptanol | 30864 | 24213 | 6651 | 27538 |
| Octanol | 30395 | 23866 | 6529 | 27130 |
| Nonanol | 34722 | 24271 | 10451 | 29496 |
| Decanol | 31347 | 24213 | 7134 | 27780 |

(a)

| **Solvents** | $\bar{\nu}_a$ | $\bar{\nu}_f$ | $\bar{\nu}_a - \bar{\nu}_f$ | $\left(\frac{\bar{\nu}_a + \bar{\nu}_f}{2}\right)$ |
|---|---|---|---|---|
| Methanol | 37174 | 24691 | 12483 | 30932 |
| Ethanol | 36363 | 24937 | 11426 | 30650 |
| Propanol | 31847 | 24813 | 07034 | 28830 |
| Butanol | 35971 | 24630 | 11341 | 30333 |
| Pentanol | 32051 | 25062 | 07439 | 28781 |
| Hexanol | 35971 | 24875 | 11096 | 30423 |
| Heptanol | 3125 | 24154 | 21029 | 13639 |
| Octanol | 3125 | 24509 | 21384 | 13817 |
| Nonanol | 35587 | 2500 | 33087 | 19043 |
| Decanol | 35971 | 24813 | 11158 | 30392 |

(b)

Table 1 (a) and (b) display the wavenumber "of absorption and emission along Stoke shift and arithmetic Stoke shift value respectively. From Fig. 3 (a), (b), and (c), its follows that, $\bar{\nu}_a - \bar{\nu}_f$ v/s $F_1(\mathcal{E}, n)$, $F_2(\mathcal{E}, n)$ and $\left(\frac{\bar{\nu}_a + \bar{\nu}_f}{2}\right)$ versus $F_3(\mathcal{E}, n)$ need to be linear, with corresponding slopes of m1, m2, and m3. 'a' denotes solute derivative's radius and value was measured employing J. T. Edwards' molecular volume increment technique. Graphs of $\bar{\nu}_a - \bar{\nu}_f$ v/s $F_1(\mathcal{E}, n)$, $F_2(\mathcal{E}, n)$ and $\left(\frac{\bar{\nu}_a + \bar{\nu}_f}{2}\right)$ versus $F_3(\mathcal{E}, n)$ are displayed in Fig. 3. Table

3 contains correlation factor, slope, & no. of" data. Each case is identified with favorable correlation factors. The quantum calculation provided value of (g), "experimental value of electric dipole moment ($\mu_g$) and excited value of electric dipole moment ($\mu_e$) calculated by employing the equations (13 & 14). The values of the dipole moment of ground and excited electric ratio and the dipole moment change ($\Delta\mu$) are mentioned in Table 2. It is found that the dipole moments of the excited state are larger than those of the ground state. It is clear from Table 3 that the dipole moment of both derivatives is greater in the first excited state than it is in the ground state. Upon" excitation, dipole moment nearly doubles. As an outcome of "ICT," this implies that a more relaxed condition is present [36-40].

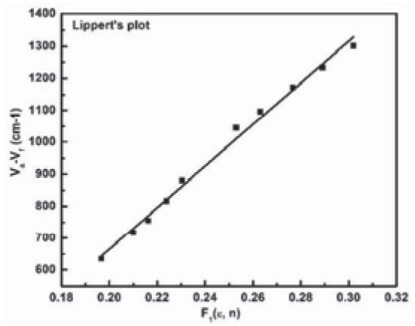


(a)

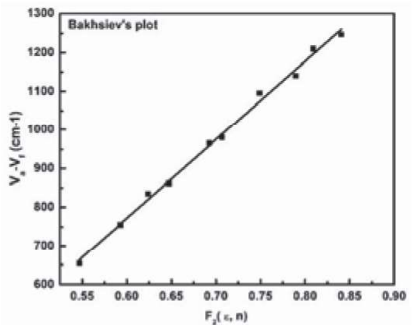


(b)

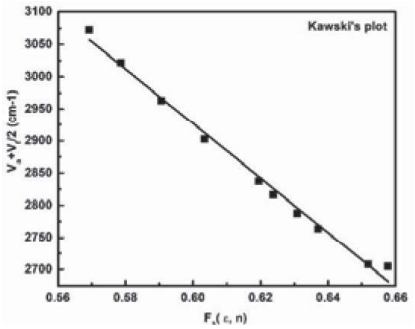


(c)

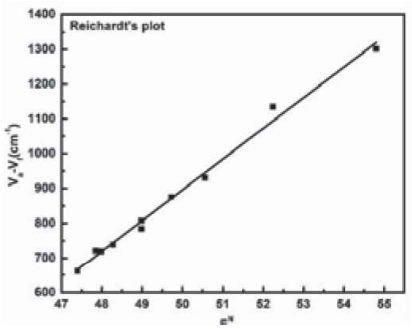


(d)

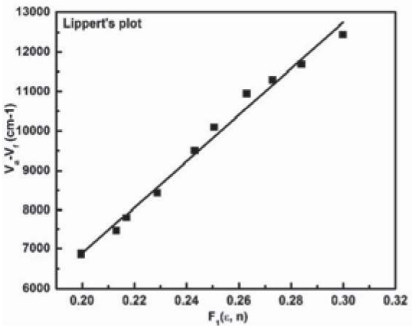


(a)

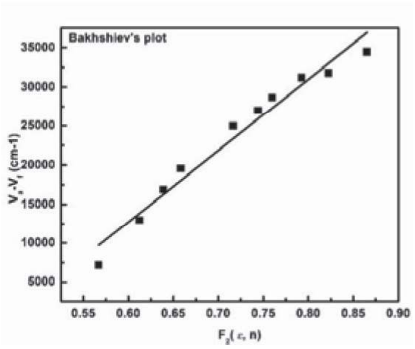


(b)

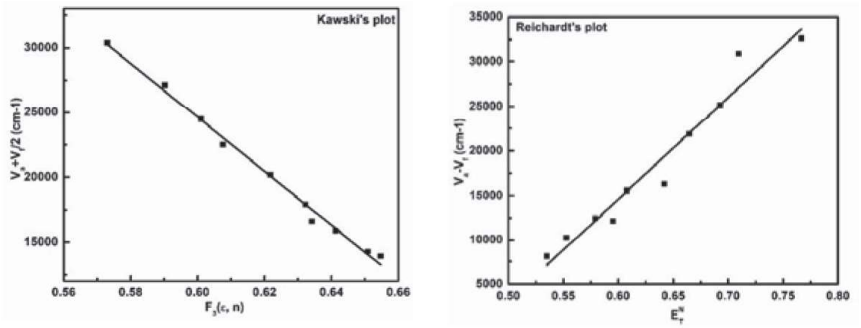


(c) (d)

**Figure 4:** Variation of stoke's shifts with polarity functions, (a) Lippert, (b) Kawski-Chamma- Viallet's and (d) Microscopic solvent polarity ($E_T^N$) functions for MPIC & CPIC.

## 4.2. Molecular-Microscopic Solvent Polarity Parameter ($E_T^N$)

The "plot of the Stokes shift for both derivatives in different solvents as a function of the microscopic solvent polarity parameter ($E_T^N$) is shown in Figure 3(d). Stokes shift's observed linear dependence on $E_T^N$ suggests a broad solute–solvent interaction in" which "the dielectric constant and solvent's refractive index both affect the shift. Table 2 summarizes the values obtained from applying Eq. (16) to the $E_T^N$ parameter for computing excited-state dipole moment μ_e^g . Remarkably, the excited-state dipole moments evaluated from ($E_T^N$) approach are marginally greater than those derived using the Bakshiev and Kawaski–Chamma-Viallet equations. This discrepancy might occur because the ($E_T^N$) technique takes into consideration the molecular aspects of solvation, but it overlooks some solute–solvent interactions such hydrogen bonding and complex formation. Intramolecular charge transfer (ICT) is confirmed by a bathochromic (red) shift seen in both the emission and absorption bands when solvent polarity increases. This suggests that, as opposed to less polar ground state with mostly mesmeric structure, excitation results in creation of a highly dipolar excited state with a dominant nitro-phenoxy-methyl structure. In accordance with ICT behavior, the excited state is therefore more polar than ground" state [41–45].

**Table 2:** Ground state and excited state dipole moments of MPIC and CPIC

| Molecular name | Radius 'a'(Å) | Slope | Dipole moments | | | | | | |
|---|---|---|---|---|---|---|---|---|---|
| MPIC | 3.60 | m = 88.20<br>$m_1$ =6504<br>$m_2$=2032<br>$m_3$=-4243 | $\mu_g^a$ | $\mu_e^b$ | $\mu_e^c$ | $\mu_e^d$ | $\mu_e^e$ | $\mu_e^f$ | $\mu_e^g$ |
| | | | 1.67 | 4.74 | 7.16 | 4.74 | 4.73 | 3.07 | 0.35 |
| CPIC | 3.58 | m=11444<br>$m_1$ =5870<br>$m_2$=9125<br>$m_3$ =-20833 | 13.1 | 33.5 | 29.4 | 33.5 | 33.4 | 20.4 | 12.5 |

1Debye (D) = $3.33564X10^{-30}$cm = $10^{-18}$ esu cm.

[a]The ground states dipole moments calculated using Equation. (10)

[b]The excited state dipole moment calculated by Equation. (11)

[c]The experimental excited state dipole moments calculated from Lippert's equation.

[d]The experimental excited state dipole moments calculated from Bakhshiev's equation.

[e]The experimental excited state dipole moments calculated from Chamma-Viallet's equation.

[f]The change in dipole moments from Equation (10) and (11).

[g]The change in dipole moments calculated from Equation (12).

## 4.3. Computational analysis

Ground-state optimizations of the synthesized dyes were performed "using DFT and TD-DFT at B3LYP/6-31G level of theory, combined with the integral equation formalism variant of the polarizable continuum model (IEFPCM) for accounting for solvation effects. Optimized molecular geometries and dipole moment directions of both molecules are illustrated in Figure 5. Ground-state dipole moments of molecules in gas phase and in various solvents were theoretically estimated employing DFT at the B3LYP/6-31G level, and findings are concluded in Table 3. The dipole moment values attained from ab initio calculations were found to be higher than those derived from experimental measurements. Additionally, the three-dimensional plots of the HOMO as well as LUMO for the synthesized fluorescent dyes are depicted in Figure 5. The computed HOMO & LUMO energy levels, along with the corresponding HOMO–LUMO energy gaps (ΔE), are represented in" Table 3 [46–47].

## 4.4. Global chemical reactivity descriptor (GCRD) parameters

To evaluate the reactivity and stability of the fluorophores, the "global chemical reactivity descriptors (GCRDs) were calculated utilizing equations (4–8) [31]. These comprised chemical softness (S), chemical hardness (η), electronegativity (χ), chemical potential (μ), and the electrophilicity index (ω).

$$\eta = (IP-EA)/2 \quad (14)$$

$$\mu = -\chi \quad (15)$$

$$\chi = (IP+EA)/2 \quad (16)$$

$$S = 1/2\eta \quad (17)$$

$$\omega = \mu^2/2\eta \quad (18)$$

where IP = $-E_{HOMO}$ is the ionization potential and EA = $-E_{LUMO}$ is the electron affinity of the molecule. The GCRD parameters for both fluorophores are shown in Table 7.

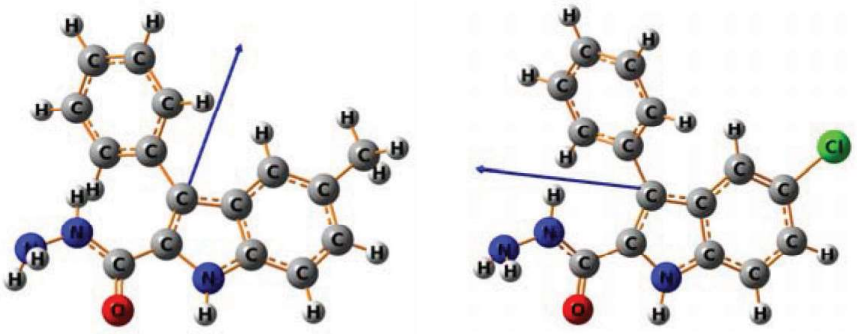

(a) (b)

**Figure 5:** Ground-state optimized molecular geometries along with the direction of dipole moment.

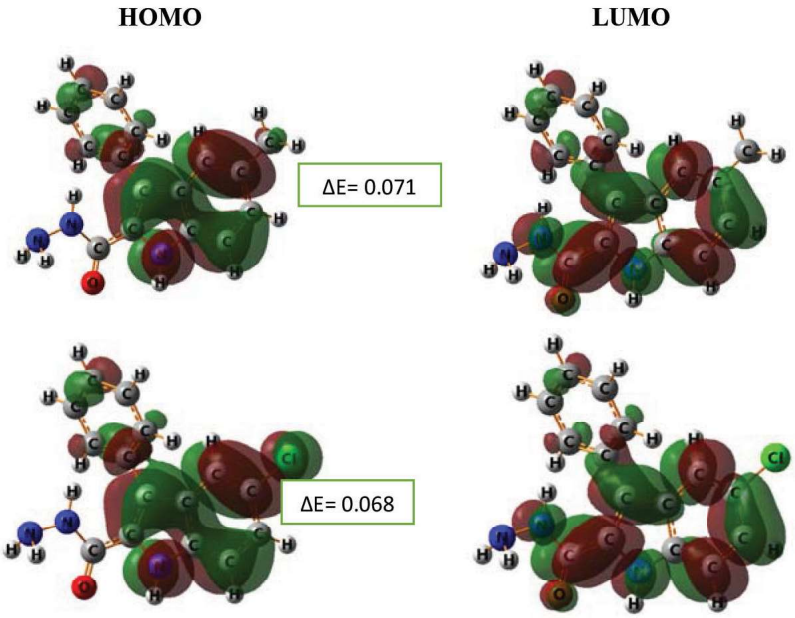


**Figure 6:** HOMO - LUMO Energy gap of MPIC and CPIC

**Table 3:** GCRD parameters of MPIC and CPIC calculated at the (B3LYP/6-31G(d)) level of theory.

| Parameter | MPIC | CPIC |
|---|---|---|
| HOMO | -0.151 | -0.158 |
| LUMO | -0.080 | -0.090 |
| IP (eV) | 0.151 | 0.158 |
| EA (eV) | 0.080 | 0.090 |
| χ (eV) | 0.116 | 0.124 |
| μ (eV) | -0.116 | -0.124 |
| η (eV) | 0.035 | 0.034 |
| S ($eV^{-1}$) | 14.15 | 14.64 |
| ω (eV) | 0.190 | 0.226 |

Molecular electrostatic surface potential (MESP) maps for both fluorophores were generated using the DFT-B3LYP/6-31G(d) method and are demonstrated in Figure 7. These maps display a color gradient ranging from red to dark blue, representing the most negative and most positive electrostatic potential regions, respectively. The overall color sequence (red, yellow, green, light blue, dark blue) reflects the transition from highly electron-rich areas (red) to highly electron-deficient areas (dark blue). Yellow regions indicate slightly less negative potential than red, light blue represents moderately positive regions, and green areas correspond to nearly neutral potential. The MESP analysis provides valuable information on the preferred sites for nucleophilic and electrophilic attack, as well as possible hydrogen-bonding" interaction sites. Both fluorophores show well-defined nucleophilic and electrophilic regions, supporting their potential reactivity patterns [48–50].

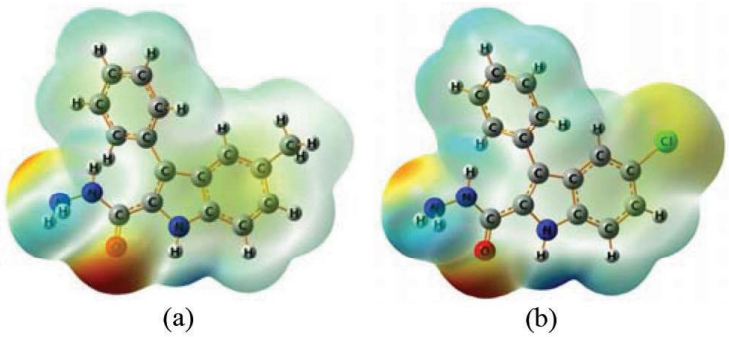


**Figure 7:** Molecular electrostatic potential map of MPIC and CPIC

## 5. Conclusions

The photophysical behaviour of the newly synthesized indole derivatives was investigated using "steady-state absorption and fluorescence emission spectroscopy. Ground-state dipole moments were determined through both experimental measurements and theoretical calculations, with the experimental values discovered to be more than theoretical predictions. Excited-state dipole moments, calculated utilizing multiple solvatochromic equations, were of comparable magnitude across methods and consistently greater than the ground-state values, highlighting that the derivatives are more polar in their excited state. The energy band gap values obtained from" experimental and theoretical approaches showed good agreement, validating the computational methodology. In addition, GCRD parameter calculations and MESP mapping confirmed the presence of distinct electrophilic and nucleophilic regions in the molecules. Collectively, these findings demonstrate that the synthesized indole derivatives are promising candidates for applications in solar energy conversion, fluorescent probes, and chemo sensor technologies.

## Reference


[1]. Lakhdar S, Westermaier M, Terrier F, Goumont R, Boubaker T, Ofial AR, Mayr H (2006) Nucleophilic reactivities of indoles. J Org Chem 71:9088–9095

[2]. Sharma V, Pradeep K, Devender P (2010) Biological importance of the indole nucleus in recent years: a comprehensive review. J Heterocycl Chem 47:491–502

[3]. Kaushik NK, Kaushik N, Attri P, Kumar N, Kim CH, Verma AK, Choi EH (2013) Biomedical Importance of Indoles. Molecules 18:6620–6662

[4]. Xue-Hua Zhang, Yan Cui, Ryuzi Katoh, Nagatoshi Koumura and Kohjiro Hara J. Phys. Chem. C 2010, 114, 42, 18283–18290

[5]. Mathada.B S, Yernale.N G, Basha J. N, J. Badiger, An insight into the advanced synthetic recipes to access ubiquitous indole heterocycles, Tetrahedron Letters, Volume 85, 2021, 153458, https://doi.org/10.1016/j.tetlet.2021.153458.

[6]. Yernale N. G, Mruthyunjayaswamy B. H. M, Metal (II) complexes of ONO donor Schiff base ligand as a new class of bioactive compounds containing indole core: Synthesis and characterization, Int J Pharm Pharm Sci, Vol 8, Issue 1, 197-204 (2016).

[7]. Hintz. T, Matthews K. K, Di. R, Biomedical Research Institute, pp.246, 2015.

[8]. Reichardt. C, Welton. T, Solvents and solvent effects in organic chemistry, John Wiley & Sons, 2011.

[9]. Ravi.M, Soujanya.T, Samanta.A, Radhakrishnan.T. P, Excited-state dipole moments of some Coumarin dyes from a solvatochromic method using the solvent polarity parameter, ENT, J. Chem. Soc., Faraday Trans. 91 (17) (1995) 2739–2742.

[10]. Reichardt. C, Solvatochromic dyes as solvent polarity indicators, Chemical reviews 94 (8) (1994) 2319–2358..

[11]. Suppan. P, Excited-state dipole moments from absorption/fluorescence solvatochromic ratios, Chem. Phys. Lett. 94 (3) (1983) 272–275, https://doi.org/10.1016/0009-2614(83)87086-9.

[12]. Edward. J. T, Molecular volumes and the Stokes-Einstein equation, J. Chem. Educ. 47 (4) (1970) 261, https://doi.org/10.1021/ed047p261

[13]. Kumar. N, Paramasivam. M, Kumar. J, Gusain. A, Hota.P. K, Tuning of optical properties of p-phenyl ethenyl-E-furans: a solvatochromism and density functional theory, Spectrochim. Acta Part A Mol. Biomol. Spectrosc. 206 (2019) 396–404, https://doi.org/10.1016/j.saa.2018.08.032.

[14]. Srinath, Chillargikar, S., Patil, O. *et al.* Experimental and Theoretical Approach to Estimate Electric Dipole Moments and Analysis of Preferential Solvation, Fluorescence Quenching of 4NPMB Coumarin Molecule by Steady State Method. *J Fluoresc* (2025). https://doi.org/10.1007/s10895-025-04331-w.

[15]. Srinath, Patil, O., Devar, S. *et al.* Estimation of Electric Dipole Moment by Solvatochromism, Computational Method, and Study of the Effect of Solvents by Preferential Solvation of 6 – Methoxy—4— (4—Nitro—Phenoxy Methyl)—Chromen—2—One (6mnpm). *J Fluoresc* **35**, 5861–5869 (2025). https://doi.org/10.1007/s10895-024-03955-8

[16]. Hanagodimath. S. M, Chikkur. G. C, Gadaginamath. G. S, Environmental effects on the energy migration coefficient, the effective energy transfer and quenching distances in an organic liquid scintillator, Chem. Phys. 148 (2) (1990) 347–357, https://doi.org/10.1016/0301-0104(90)89030-T.

[17]. Hanagodimath. S. M, Chikkur. G. C, Gadaginamath. G. S, ''Role of Brownian diffusion and interaction distance on energy transfer and quenching in an organic liquid scintillator, Int. J. Radiat. Appl. Instrument. Part A. Appl. Radiat. Isotopes 41 (9) (1990) 817–821, https://doi.org/10.1016/0883-2889(90) 90058-O

[18]. Hanagodimath. S. M, Chikkur. G. C, Gadaginamath. G. S, An unique method of determining the excitation energy migration coefficient in organic liquid scintillators, Pramana – J. Phys. 37 (2) (1991) 153–161, https://doi.org/ 10.1007/BF02875302.

[19]. Hanagodimath. S. M, Chikkur. G. C, Gadaginamath. G. S, On the mechanism of excitation energy transfer involving long and short range interaction in dilute organic liquid scintillator systems, Acta Phys. Pol. A 81 (3) (1992) 361–368.

[20]. Melavanki. R, T. Muttannavar, S. Vaijayanthimala, N. Patil, L. Naik, J. Kadadevarmath, Solvent effects on the dipole moments and photo physical properties of laser dye, Indian J. Pure Appl. Phys. 56 (2018) 749–754.

[21]. Desai. V. R, Hanagodimath.S.M, Basanagouda.M, Kadadevarmath.J.S, Thipperudrappa.J, Sidarai.A.H, Spectroscopic studies on newly synthesized 5- (2-hydroxy-5-methoxy-phenyl)-2-phenyl-2H-pyridazin-3-one molecule, J. Mol. Liq. 225 (2017) 613–620, https://doi.org/10.1016/j.molliq.2016.11.080.

[22]. Desai. V. R, Hanagodimath.S.M, Basanagouda.M, Kadadevarmath.J.S, Thipperudrappa.J,Sidarai.A.H, Solvent effects on the electronic absorption and fluorescence spectra of HNP: estimation of ground and excited state dipole moments, J. Fluoresc. 26 (4) (2016) 1391–1400, https://doi.org/10.1007/ s10895-016-1830-3.

[23]. Siddlingeshwar. B, Hanagodimath.S.M, Kirilova. E. M, Kirilov. G.K, Photophysical characteristics of three novel benzanthrone derivatives: Experimental and theoretical estimation of dipole moments, J. Quant. Spectrosc. Radiat. Transfer 112 (3) (2011) 448–456, https://doi.org/10.1016/j. jqsrt.2010.09.00.

[24]. Mathapati.G. B, Ingalgondi.P.K, Patil.O, Basavaraj.S, Hanagodimath.S.M, Estimation of ground and excited state dipole moments of newly synthesized coumarin molecule, Int. J. Scient. Res. Phys. Appl. Sci. 5 (2018) 1061–1065.

[25]. Mathapati.G.B, Patil.O, Basavaraj.S, Gounalli.S, Hanagodimat.S.M, Estimation of ground and excited state dipole moments of newly synthesized coumarin molecule by Solvatochromic shift method and Gaussian software, Int. J. sci. Res. Phys. Appl. Sci. 7 (2019) 38–43, https://doi.org/10.26438/ijsrpas/ v7i2.3843.

[26]. Kulkarni MV, Kulkarni GM, Lin CH, Sun CM (2006) Recent advances in coumarins and 1-azacoumarins as versatile biody namic agents. Curr Med Chem 13:2795–2818.

[27]. Patil O, Ingalagondi PK, Hanagodimath SM (2021) Estimation of dipole moments of new coumarin dye by experimental and theoretical methods. Macromol Symp 400:2100015. https:// doi. org/10.1002/masy.202100015.

[28]. Lipert.E, Dipole moment and electronic structure of excited molecules, Z. Naturforsch 10 (1955) 541–546.

[29]. Mataga.N, Kaifu.Y, Koizumi.M, The solvent effect on fluorescence spectrum, change of solute-solvent interaction during the lifetime of excited solute molecule, BCSJ 28(9) (1955)690https://doi.org/10.1246/bcsj.28.690.

[30]. Bakshiev.N.G, Solvent dielectric relaxation effects, Optical Spectroscopy" 13 (1962) 507–530.

[31]. Bilot.L, Kawski.A, Zur theorie des einflusses von Lösungsmitteln auf die elektronenspektren der moleküle, Zeitschrift für Naturforschung A 17 (7) (1962) 621–627.

[32]. Bilot.L,Kawski.A,Der Einfluß des Lösungsmittels auf die Elektronenspektren lumineszierender Moleküle, Z. Naturforsch 18A (1963) 10–15.

[33]. Pourtabrizi.M, Shahtahmassebi.N, Kompany.A, Sharifi.S, Dipole moment of excited and ground state of Auramine O doped nano-droplet, Opt. Quant. Electron. 49 (9) (2017) 291, https://doi.org/10.1007/s11082-017-1124-2.

[34]. Reichardt.C, Welton.T, Solvents and solvent effects in organic chemistry, John Wiley & Sons, 2011.

[35]. Ravi.M, Soujanya.T, Samanta.A, Radhakrishnan.T.P, Excited-state dipole moments of some Coumarin dyes from a solvatochromic method using the solvent polarity parameter, ENT, J. Chem. Soc., Faraday Trans. 91 (17) (1995) 2739–2742.

[36]. Reichardt.C, Solvatochromic dyes as solvent polarity indicators, Chemical reviews 94 (8) (1994) 2319–2358..

[37]. Suppan.P, Excited-state dipole moments from absorption/fluorescence solvatochromic ratios, Chem. Phys. Lett. 94 (3) (1983) 272–275, https://doi. org/10.1016/0009-2614(83)87086-9.

[38]. Edward.J.T, Molecular volumes and the Stokes-Einstein equation, J. Chem. Educ. 47 (4) (1970) 261, https://doi.org/10.1021/ed047p261.

[39]. Kumar.N, Paramasivam.M, Kumar.J, Gusain.A, Hota.P.K, Tuning of optical properties of p-phenyl ethenyl-E-furans: a solvatochromism and density functional theory, Spectrochim. Acta Part A Mol. Biomol. Spectrosc. 206 (2019) 396–404, https://doi.org/10.1016/j.saa.2018.08.032.

[40]. Desai.V.R, Hanagodimath.S.M, Basanagouda.M, Kadadevarmath.J.S, Thipperudrappa.J, Sidarai.A.H, Spectroscopic studies on newly synthesized 5- (2-hydroxy-5-methoxy-phenyl)-2-phenyl-2H-pyridazin-3-one molecule, J. Mol. Liq. 225 (2017) 613–620, https://doi.org/10.1016/j.molliq.2016.11.080.

[41]. Kumari.R, Varghese.A, George.L, Synthesis, crystal structure and photophysical properties of (E)-4-(4-(2-hydroxybenzylideneamino) benzyl) oxazolidin-2-one, J. Lumin. 179 (2016) 518–526.

[42]. Patil.S.N, Sanningannavar.F.M, Navati.B.S, Patil.N.R, Kusanur.R.A, R.M.Melavanki, Spectroscopic properties and estimation of ground and excited state dipole moments of biologically active fluorescent molecule from absorption and emission spectra 4 (1) (2014) 11.

[43]. Sharifi.S, Salavatovna.S.G, Azarpour.A, Rakhshanizadeh.F, Zohuri.G, Sharifmoghadam.M.R, Optical properties of methyl orange-doped droplet and photodynamic therapy of Staphylococcus aureus, J. Fluoresc. 29 (6) (2019) 1331–1341, https://doi.org/10.1007/s10895-019-02459-0.

[44]. Desai.V.R, Hanagodimath.S.M, Basanagouda.M, Kadadevarmath.J.S, Sidarai.A.H, Solvent effects on the electronic absorption and fluorescence spectra of HNP: estimation of ground and excited state dipole moments, J. Fluoresc. 26 (4) (2016) 1391–1400, https://doi.org/10.1007/s10895-016-1830-3.

[45]. Pujar.G.H, Wari.M.N, Steffi.B, Varsha.H, Kavita.B, Panicker.Y.C, Santhosh.C, Ajeetkumar.P, Inamdar.S.R, A combined experimental and computational investigation of solvatochromism of nonpolar laser dyes: Evaluation of ground and singlet excited-state dipole moments, J. Mol. Liq. 244 (2017) 453–463, https://doi.org/10.1016/j.molliq.2017.08.078.

[46]. Siddlingeshwar.B, Hanagodimath.S.H, Kirilova.E.M, Kirilov.G.K, Photophysical characteristics of three novel benzanthrone derivatives: Experimental and theoretical estimation of dipole moments, J. Quant. Spectrosc. Radiat. Transfer 112 (3) (2011) 448–456, https://doi.org/10.1016/j.jqsrt.2010.09.00.

[47]. Mathapati.G.B, Ingalgondi.P.K, Patil.O, Basavaraj.S, Hanagodimath.S.M, Estimation of ground and excited state dipole moments of newly synthesized coumarin molecule, Int. J. Scient. Res. Phys. Appl. Sci. 5 (2018) 1061–1065.

[48]. Mathapati.G.B, Ingalgondi.P.K, Patil.O, Basavaraj.S, Hanagodimath.S.M, Estimation of ground and excited state dipole moments of newly synthesized coumarin molecule by Solvatochromic shift method and Gaussian software, Int.J.sci.Res.Phys Appl.Sci.7(2019) 38–43, https: //doi.org /10.26438 /ijsrpas / v7i2. 3843.

[49]. Sidir.Y.G, The solvatochromism, electronic structure, electric dipole moments and DFT calculations of benzoic acid liquid crystals, Liq. Cryst. 47 (10) (2020) 1435–1451, https://doi.org/10.1080/02678292.2020.1733685.

[50]. Pandey.N, Tewari.N, Pant.S, Mehata.M.S, Solvatochromism and estimation of ground and excited state dipole moments of 6-aminoquinoline, Spectrochim.